RSC Advances

PAPER

View Article Online
View Journal | View Issue

Cite this: *RSC Adv.*, 2014, **4**, 53157

Photocatalytic reactions of a nickel(II) annulene complex incorporated in polymeric structures†

G. Estiu,‡[a] G. Ferraudi,*[b] A. G. Lappin,*[a] G. T. Ruiz,*[c] C. Vericat,[c] J. Costamagna[d] and M. Villagran[d]

Received 6th August 2014
Accepted 7th October 2014

DOI: 10.1039/c4ra08177c

www.rsc.org/advances

The photochemical reactions of the Ni(II) annulene complex, [Ni^{II}([5,7,12,14]-tetra methyl dibenzo[2,3-*b*:2,3-*b*,*i*][1,4,8,11]tetraaza[14]annulenate)], grafted into a poly(isobutylene-*alt*-maleate) backbone were investigated in aqueous media. The grafted Ni(II) complex becomes soluble in aqueous and organic solvents where the strands form aggregates with medium-dependent shapes. Irradiation of the polymer at 532 or 351 nm produce charge-separated macrocyclic pendants, CS, with a lifetime $\tau \sim 30$ ns. CS reacts with electron donors and acceptors before it decays with a lifetime $\tau \sim 1$ μs. In parallel to the decay of CS, an excited state-excited state annihilation process gives rise to luminescence whose spectrum spans wavelengths shorter than the wavelength of the irradiation, $\lambda_{ex} > 500$ nm. Theoretical calculations were carried out with the aim of understanding the morphology and structures of strand aggregates, to confirm the nature of reaction products and to account for the spectroscopic and photochemical properties of the Ni(II) pendants. The endothermic reduction of CO_2 to CO by S(IV) species was used as a test of the Ni(II) complex's ability to photocatalyze the reaction. In the photoprocess, the Ni(II) complex fulfills the double role of antenna and catalyst.

Introduction

Transition metal coordination complexes grafted into a polymer backbone have an extensive and diverse chemistry that can be useful for practical applications.[1] Processes such as the photo-induced oxidative degradation of lignin[2] and the reduction of CO_2 to CO (this work) can be applied to the photoproduction of strategic materials and the storage of solar energy. Among the transition metal complexes capable of catalyzing thermal and photochemical reactions, complexes of the dinaphtoannulene ligands, Scheme 1 top, deposited on electrodes catalyze electrochemical reactions such as the reductions of H_2O and CO_2.[3]

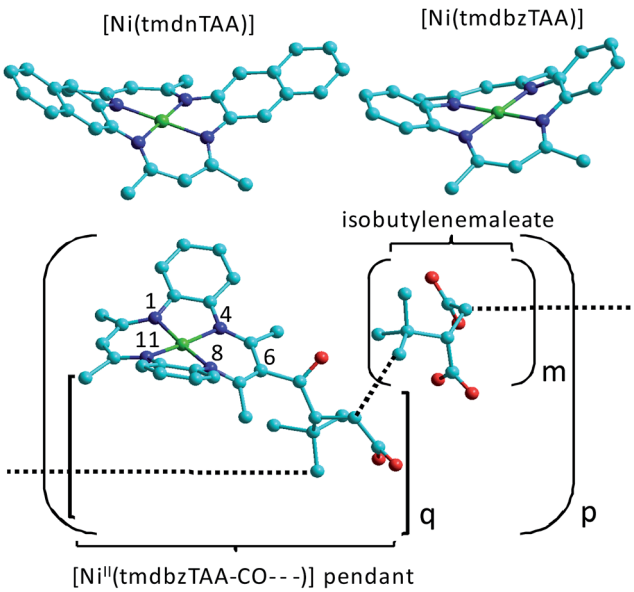

poly(Ni[tmdbzTAA])$_1$: q = 1, m = 5; p = 78

poly(Ni[tmdbzTAA])$_2$: q = 2, m = 5; p = 67

Scheme 1 Structure of the free complexes (top) and average structures of the poly[Ni^{II}(tmdbzTAA)]$_n$ polymers with C, N, O, Ni; H atoms are not shown.

[a]*Department of Chemistry, Univ. of Notre Dame, Notre Dame, IN 46556, USA*
[b]*Department of Chemistry, Radiation Research Building, Univ. of Notre Dame, Notre Dame, IN 46556, USA. E-mail: ferraudi.1@nd.edu*
[c]*Instituto de Investigaciones Fisicoquímicas Teóricas y Aplicadas (INIFTA, UNLP, CCT La Plata-CONICET), Diag. 113 y 64, Sucursal 4, C.C. 16, B1906ZAA La Plata, Argentina*
[d]*Faculty of Chemistry and Biology, Universidad de Santiago de Chile, Santiago, Chile*

† Electronic supplementary information (ESI) available: Fig. S1 with spectroscopic properties of poly(Ni[tmdbzTAA])$_2$. (a): NMR spectrum in dimethylsulfoxide-d$_6$ and (b and c): FTIR in solid phase. Fig. S2 with GC chromatogram of photolysis products of the CO_2 reduction. Fig. S3 with TEM and AFM observations of poly(Ni[TMBzTAA])$_2$ in aqueous CH_3CN. Fig. S4 with TEM and AFM observations of poly(Ni[TMBzTAA])$_2$ in basic solutions. Fig. S5 with voltammetric responses of poly(Ni[TMBzTAA])$_2$ in *N*,*N*′-dimethylformamide. A movie (3chains.wmv) with the molecular mechanics calculation of the motions of three strands fragments. See DOI: 10.1039/c4ra08177c

‡ This work is dedicated to G. E who passed away on 5/9/2014.

However, applications of the annulene complexes to homogeneous catalysis are limited by poor solubility in polar and aqueous solvents. Formation of a water soluble polyelectrolyte where the annulene complexes are grafted can impart upon the complex enhanced solubility in water.[2,4–6] To this aim, two new compounds, poly(Ni^{II}[tmdbzTAA])$_n$, formed when different proportions of the annulene complex, [Ni(tmdbzTAA)], tmdbTAA = [5,7,12,14]-tetramethyldibenzo [2,3-*b*:2,3-*b*,*i*] [1,4,8,11]tetraaza[14] annulenate^{2-}, were grafted into a poly-(isobutylene-*alt*-maleic anhydride) backbone, Scheme 1 bottom. The large solubility in water of the nickel(II) complex, present now as pendants in the polycarboxylate backbone, allows to investigate previously inaccessible thermal, electrochemical and photochemical reactions of the grafted nickel(II) complex in this medium. For example, the migration of energy and charge through the Ni(II) pendant-crowded arrangements in a strand or bundle of strands becomes accessible under much more gentle conditions than those required in solutions of the polymer free [Ni(tmdbzTAA)] complex. Also in the present work, the strategy we have used is to adapt this chemistry to a homogeneous system better suited to photocatalysis. Such water-soluble homogeneous photocatalyst consists of a nickel(II) naphtho-annuleno complex grafted into a polymer backbone. The applicability of these systems to the reduction of CO_2 to CO should be highlighted as the most relevant result of this research. The endothermic reduction of CO_2 to CO by HSO_3^-/SO_3^{2-} where the grafted nickel(II) complex has the dual role of an antenna and a catalyst is used as a test of the complex catalytic capability. The reaction, eqn (1), as written is thermodynamically disfavoured by +186.36 kJ mol^{-1}.

$$SO_2(g) + CO_2(g) \rightarrow SO_3(g) + CO(g) \quad (1)$$

This energetic deficit corresponds to a wavelength for photoactivation of 642 nm. In aqueous solution at pH = 8, the appropriate reaction, is also disfavoured but with a smaller energy deficit, ≥70 kJ mol^{-1}, eqn (2).

$$SO_2(aq.) + CO_2(aq.) + H_2O \rightarrow SO_4^{2-}(aq.) + CO(g) + 2H^+(aq.) \quad (2)$$

Consequently, this reaction can be photo-activated with visible light with a catalytic reagent that incorporates an absorption antenna. Under these conditions, poly(Ni^{II}[tmdbzTAA])$_n$, becomes a catalyst of practical importance, useful for storage of energy.

Experimental

General methods and techniques

TEM and AFM methodologies combined with various spectroscopies (UV-Vis-NIR, NMR) were applied to the structural and morphological studies of the polymers Analytical protocols, the methods and apparatuses used in cyclic voltammetry, pulse radiolysis, flash and steady state photolysis were previously described.[7–22] Detailed descriptions of the experimental methods and techniques are given in the ESI.†

Materials

The Ni^{II}[tmdbzTAA] was prepared and purified by a published procedure.[23] Aldrich poly(isobutylene-*alt*-maleic anydride), Mw = 10^4, was used as received.

Different procedures for the grafting of transition metal complexes into preformed polymers have been described in the literature.[24] One, leading to the formation of covalent bonds between the polymer and the ligand, has been applied to the syntheses of poly(Ni^{II}[tmdbzTAA]).

Poly(Ni^{II}[tmdbzTAA])$_1$ (Scheme 1)

Poly(isobutylene-*alt*-maleic anhydride), 3.9 g (25 mmol of poly-(isobutylene-*alt*-maleic anydride) repeating units), was added to 200 mL of DMF under N_2 and the mixture was stirred for at least 1/2 h until a complete dissolution of the polymer was accomplished. A solution of Ni(tmdbzTAA), 2.0 g (5 mmol) in 100 mL of DMF was added to the former solution and stirred an additional 1/2 h before the dropwise addition of 6 mL of tEA (tEA = triethylamine). The temperature of the resulting solution was gradually raised to 65 ± 5 °C while it was stirred under N_2 and kept 16 h at this temperature. A crude product was obtained after rotoevaporation of the liquid at 55 °C under a 1 Torr pressure. About 1 g of this solid was dissolved in 50 cm^3 of 0.1 M NaOH. The concentrated solution was loaded in a 3.3 cm diameter and 40 cm high (340 mL volume) C10-Sephadex column and several fractions were eluted with H_2O. The solid product obtained from rotovaporating at 45 °C the first fraction eluted from the column was a partially protonated hydrate. Anal. calcd for the repeating unit, ($NiC_{29}N_4H_{30}O_3Na$)–($C_7H_8O_4Na_2$)$_2$($C_7H_8O_4H_2$)$_3H_2O$ (≡ $NiC_{64}N_4H_{78}O_{24}Na_5$): H, 5.38; C, 52.62; N, 3.83. Found: H, 5.47; C, 53.30; N, 3.38. The hydrate was dissolved in 50 cm^3 of H_2O titrated to pH = 8 with 1 M NaOH, loaded into the C-10 Sephadex column and eluted with H_2O. The solid obtained after rotovaporation of the first fraction at 45 °C was dried under vacuum for 72 h at 30 °C. Anal. calcd for the repeating unit, ($NiC_{29}N_4H_{30}O_3Na$)($C_7H_8O_4Na_2$)$_5$($NiC_{64}N_4H_{70}O_{23}Na_{11}$): H, 4.48; C, 48.81; N, 3.56. Found: H, 4.70; C, 49.30; N, 3.35. Additionally, a 3.8% Ni content was determined after the mineralization of the compound. The formula weight, FW = 1.5 × 10^3, of the repeating unit, calculated from the Ni content and the formula weight, FW = 1.6 × 10^3, and one calculated for the formula ($NiC_{29}N_4H_{30}O_3Na$)($C_7H_8O_4Na_2$)$_5$ are in good agreement.

Poly(Ni^{II}[tmdbzTAA])$_2$ (Scheme 1)

Instead of the 2 g of Ni(tmdbzTAA) used in the preparation of poly(Ni^{II}[tmdbzTAA])$_1$, 5 g (10 mmol) of the Ni(tmdbzTAA) complex were used in the preparation of poly(Ni^{II}[tmdbzTAA])$_2$. Anal. calcd. for the repeating unit, ($NiC_{29}N_4H_{30}O_3Na$)$_2$($C_7H_8O_4Na_2$)$_5$ (≡ $Ni_2C_{93}N_8H_{100}O_{26}Na_{12}$): H, 4.71; C, 52.22; N, 5.24. Found: H, 4.80; C, 51.30; N, 5.35. The formula weight, FW = 1.1 × 10^3 per Ni in the repeating unit was calculated on the basis of a 5.6% Ni content. It agrees well with the formula weight, FW =

1.07×10^3 per Ni, calculated for the minimal formula $(NiC_{29}N_4H_{30}O_3Na)_2(C_7H_8O_4Na_2)_5$.

The relationships of [Ni^{II}(tmdbzTAA-CO$\cdots$)] pendants to isobutylenemaleate groups were confirmed on the basis of the C, N, H, elemental analysis. Based on the weight-average molecular weight, Mw = 10^4, of the poly(isobutylene-*alt*-maleic anydride) and the Ni contents in poly(Ni^{II}[tmdbzTAA]), n = 1, 2, it was estimated that respectively have 5 and 2.5 isobutylenemaleate units per [Ni^{II}(tmdbzTAA-CO$\cdots$)] pendant, Scheme 1. The structure and morphology of poly(Ni^{II}[tmdbzTAA])$_n$ were established on the basis of ^{1}H-NMR, FTIR, UV-Vis spectroscopic and AFM, TEM experimental observations. The TEM and AFM experimental observations are communicated together in the ESI.† For the sake of simplicity, only conclusions about the structure and morphology of poly(Ni^{II}[tmdbzTAA])$_n$ are briefly described at the beginning of the Results section. The ^{1}H-NMR spectrum of poly(Ni[tmdbzTAA])$_n$ in dimethylsulfoxide-d_6 shows resonances at 6.76–6.88, 4.90 and 2.00 ppm (labeled a in Fig. S1a†). They are assigned to the C_6H_4, CH_3 and CH groups in the macrocyclic ligand by comparison to the literature H-NMR spectrum of Ni^{II}[tmdbzTAA]. Moreover, resonances observed in a 1.0 to 2.8 ppm region, *i.e.*, those labeled b in Fig. S1a,† have been assigned to the polymer backbone. In the FTIR spectrum of the solid poly(Ni^{II}[tmdbzTAA])$_n$, n = 1, 2, various frequencies were assigned to characteristic vibrations of the [Ni^{II}(tmdbzTAA-CO$\cdots$)]pendants, Fig. S1b and c,† by comparison to the FTIR spectrum of the Ni^{II}[tmdbzTAA]. In addition to the vibrations of the pendent macrocycle, the spectrum also displays $\nu_{(C=H)}$, $\nu_{(C=O)}$ and carboxylate vibrations, typical of the polymer backbone. These experimental observations can be interpreted in terms of average structures of poly(Ni^{II}[tmdbzTAA])$_n$, n = 1, 2, shown in the Scheme 1.

Results

The poly(Ni^{II}[tmdbzTAA])$_n$, n = 1, 2 polymers have been analyzed in their structure, chemical and photochemical activity, both experimentally and computationally. The most relevant observation, for its practical importance, is the one associated with the catalytic activity for the reduction of CO_2 to CO. We discuss latter the structural, electronic and photochemical characteristics for a better understanding of the catalytic performance.

1. Photocatalyzed reduction of CO_2 to CO using HSO_3^-/SO_3^{2-} as sacrificial reagent

Poly(Ni^{II}[tmdbzTAA]), n = 1, 2 exhibited little if any differences in terms of their chemical reactions, in particular, when their concentrations were expressed as concentrations of [Ni^{II}(tmdbzTAA-CO$\cdots$)] pendants. Therefore, the experiments communicated below were mostly made with poly(Ni^{II}[tmdbzTAA])$_2$. The key observations in this paper are those that demonstrate the photocatalytic reduction of CO_2 to CO. A typical chromatographic trace of the head gasses is shown in Fig. S2.† The products were obtained after photolysis of solutions containing 20 to 30 mg of poly(Ni[tmdbzTAA])$_2$ in 20 cm^3 of a 20% or 30% (v/v) CH_3CN in H_2O mixed solvent. These solutions were placed in a gas tight photochemical cell and deaerated with a 1 : 1 molar mixture of CO_2 and SO_2. The solutions were equilibrated under 1 atm of the gas mixture and irradiated with white light, $\lambda_{ex} \geq 400$ nm, for variable periods. Chromatographic analyses of the gas produced after each irradiation period revealed that CO increased with the photolysis time. A catalyst turnover number, TON = (moles of CO produced)/(mols of [Ni^{II}(tmdbzTAA-CO$\cdots$)]), greater than 700 was calculated from the CO produced when a solution was photolyzed 120 h. Additionally, large concentrations of SO_4^{2-}, comparable to the quantities of the photogenerated CO, were detected in the photolyzed solutions. In contrast, no CO was detected when solutions with the composition indicated above were deaerated respectively with 1 : 1 molar mixtures of N_2/SO_2 and CO_2/N_2 and irradiated with white light, $\lambda_{ex} \geq 400$ nm, for 24 h.

In other experiments, a solution containing 20 to 30 mg of poly(Ni[tmdbzTAA])$_2$ in 20 cm^3 of a 20% or 30% (v/v) CH_3CN in H_2O mixed solvent was deaerated with the 1 : 1 molar of CO_2 and SO_2 and irradiated with 520 nm light for a period of 24 h. A product yield, ϕ = 0.3, was calculated from the mols of CO produced and the number of 520 nm photons absorbed by the solution.

The CO product was also detected in the white light photolysis of a solution where 20 to 30 mg of poly(Ni[tmdbzTAA])$_2$ were added to 20 cm^3 of a solution containing 0.1 M in $NaHSO_3$, 0.1 M in Na_2CO_3 and equilibrated under 1 atm of CO_2. In this condition, the CO was produced in a smaller yield than in the condition of the white-light photolysis described above.

When the reactions are carried out in the absence of CH_3CN at pH = 8, CO is also generated but the reaction extent is limited by precipitation of the catalyst when the pH decreases below pH = 6. The precipitated catalyst can be redissolved and reactivated in aqueous media at pH = 8.

2. Polymer structure, morphology and pH effects

2a. Structure and morphological study. The structures and morphologies of poly(Ni^{II}[tmdbzTAA])$_n$ (n = 1, 2), Scheme 1, have been analyzed as they impact the reaction pathways of the pendant complexes in solution.[2,4–6] Results of structural and morphological studies are detailed in the Experimental ESI sections, Fig. S3 and S4,† and are only briefly described here. In the aqueous solution phase, poly(Ni^{II}[tmdbzTAA])$_n$ (n = 1, 2) are in the form of strand aggregates with concentration- and pH-dependent morphologies. At pH 8 or 10, concentrated solutions of poly(Ni^{II}[tmdbzTAA])$_n$ (n = 1, 2) show aggregates with a globular shape that changes to an elongated and contorted morphology on dilution. By contrast, the aggregates appear as stick like structures at pH < 6, in CH_3CN–H_2O mixed media. Conversion between these morphologies takes place with a pH-dependent rate that is reflected in the protonation of the Ni(II) annulene pendants.

2b. Hindered protonation and cyclic voltammetry of the [Ni^{II}(tmdbzTAA-CO···)] pendants. The spectroscopic changes caused by the protonation of the annulene ligand in the [Ni^{II}(tmdbzTAA-CO···)] pendant and [Ni^{II}(tmdbzTAA)] complex are similar to those seen in the protonation of the [Ni^{II}(tmdbzTAA)] complex.[25] However in comparison to the prompt protonation of the [Ni^{II}(tmdbzTAA)] complex, the spectroscopic changes due to the [Ni^{II}(tmdbzTAA-CO···)] protonation are extremely slow. Solutions of poly(Ni^{II}[tmdbzTAA])$_n$, $n = 1, 2$, in a 20% (v/v) H_2O in CH_3CN mixed solvent were used for a study of the protonation of [Ni^{II}(tmdbzTAA-CO···)] pendants. A slightly basic solution containing ~1.7 mg of the polymer in 5 mL of H_2O was added to 20 mL of CH_3CN and the pH was adjusted with 11.6 M $HClO_4$. Solutions with pH = 3 and 4 were used for the spectrophotometric study of the protonation process. Changes in the solution UV-Vis spectrum take place over several days, Fig. 1. On the basis of the differences between the spectra of the protonated and deprotonated forms of [Ni^{II}(tmdbzTAA)], the observed changes in the spectrum of poly(Ni^{II}[tmdbzTAA])$_n$ are associated with the reaction of the annulene pendant with two equivalents of acid. Additionally, the protonation of the [Ni^{II}(tmdbzTAA-CO···)] is kinetically complex and dependent on the concentration of acid. For example the rate of protonation is kinetically of a zero order in polymer and acid concentrations at pH = 4, with $k = 3.3 \times 10^{-5}$ (M of [Ni^{II}(tmdbzTAA-CO···)]) min^{-1}. In contrast to the kinetics at pH = 4, several faster steps were observed when the protonation process was carried out in solutions acidified to a pH = 3. The first and faster step is kinetically of a zero order with a rate constant $k = 1.05 \times 10^{-4}$ (M of [Ni^{II}(tmdbzTAA-CO···)]) min^{-1}.

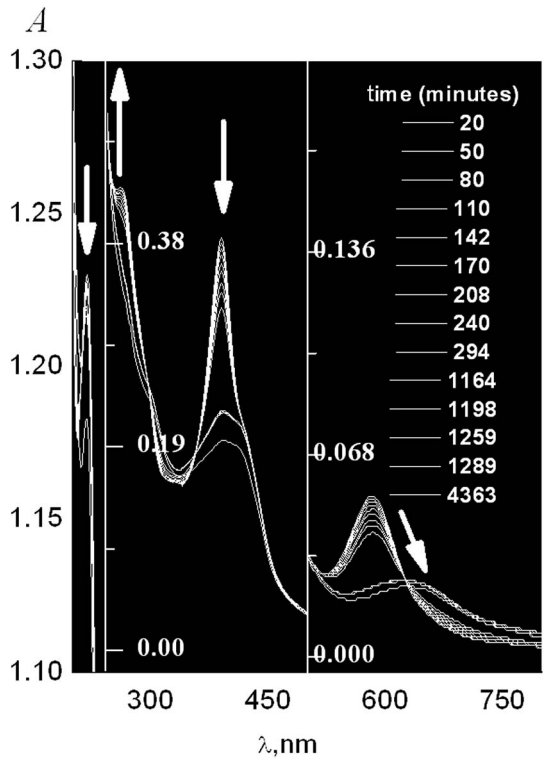

Fig. 1 Changes of the poly(Ni^{II}[tmdbzTAA])$_2$ UV-Vis absorption spectrum with time due to the annulene ligand protonation. The inset show delays (in minutes) used when each spectrum was recorded and the arrows show the sense of the change in the spectrum.

The pH-induced morphological changes are also reflected in the cyclic voltammetry of [Ni^{II}(tmdbzTAA-CO···)] pendants. A saturated solution of poly(Ni^{II}[tmdbzTAA])$_2$ in deaerated DMF, where the deprotonated globular aggregate is the most abundant, was used in a study of the nickel(II) pendants redox behavior. The voltammetric response consisted of two irreversible peaks at +0.75 V and +1.20 V *vs.* Ag/AgCl in the anodic region and an essentially irreversible peak at *ca.* −1.7 V in the cathodic region, Fig. S5.† The peaks at +0.75 V and +1.20 V are very close to those reported for the cyclic voltammogram of [Ni^{II}(tmdbzTAA)],[25–28] and have been assigned to the oxidation of the macrocyclic ligand by the successive removal of 1 and 2 electrons. A peak at −1.7 V *vs.* Ag/AgCl compares very well with that assigned to the nickel(II)/(I) couple in the [Ni^{II}(tmdbzTAA)] complex.[26]

The [Ni^{II}(tmdbzTAA-CO···)] protonation was followed by recording voltammograms for Ar-deaerated solutions of the polymer containing 4.9×10^{-4} M [Ni^{II}(tmdbzTAA-CO···)] pendants in a 20% (v/v) H_2O in CH_3CN mixed solvent with a pH = 4. The first voltammogram was recorded 2 min after the aqueous and CH_3CN solutions were mixed in the manner described in the spectroscopic study of the [Ni^{II}(tmdbzTAA-CO···)] protonation. Additional one-sweep voltammograms were successively recorded at various intervals over a period of 24 h. The irreversible waves at +0.6 and +1.1 V *vs.* SCE assigned to the successive 1 and 2 electron oxidations of the macrocyclic ligand, shifted to more positive potentials with time. The wave at +0.6 V becomes vanishingly small in those voltammograms recorded with solutions aged more than 1400 min. The displacement of the +1.1 V wave is less pronounced. The changes in the position and the intensity of the wave occur on the same timescale as changes in the optical spectrum of [Ni^{II}(tmdbzTAA-CO···)] pendants due to the ligand protonation.

Broad irreversible waves were observed in the 0 to −0.75 V cathodic sweep. They move within this range of potential and become also more defined with time. Some of the waves can be associated with covalently linked intra- and inter-strand pendant dimers formed by a one electron oxidation of the annulene ligand. A related electrochemical formation of dimers has been observed by several groups investigating the electrochemistry of [M(tmdbzTAA)], M = Cu and Ni, complexes.[26–28] The dependence of the cyclic voltammograms on time and pH suggests that the most important processes responsible of the observed changes in the voltammograms are the formation of dimers (or oligomers) of the Ni(II) pendants in conjunction with morphological transformations caused by the protonation of the polymer.

3. Electronic structure and UV-Vis spectroscopy of poly(Ni^{II}[tmdbzTAA])$_n$

UV-Vis spectroscopy was used in conjunction with theory to gain information on the nature of [Ni^{II}(tmdbzTAA-CO···)] electronic structure. The poly(Ni^{II}[tmdbzTAA])$_n$, $n = 1, 2$, polymers

exhibit similar absorption spectra with the extinction coefficients denoting the effective proportions of [Ni^{II}(tmdbzTAA-CO···)] pendants. The UV-Vis spectrum of the polymer was recorded with solutions containing concentrations of [Ni^{II}(tmdbzTAA-CO···)] pendants ranging from 4.0×10^{-4} to 3.0×10^{-5} M in neat DMF. To investigate the effect of the medium on the polymer spectrum, solutions of the polymer in 0%, 10%, 20% and 50% (v/v) CH_3CN in H_2O mixed solvents buffered at pH = 8, were also used. In all of these conditions, the spectra exhibit bands with $\lambda_{max} \sim 585$, 390 and, 335 nm and a shoulder at ~430 nm. Differences in the position of the absorption bands observed from solvent to solvent are small. Moreover the spectrum of the [Ni^{II}(tmdbzTAA-CO···)] pendants shows a close resemblance to the UV-Vis absorption spectrum of [Ni^{II}(tmdbzTAA)] in organic solvents.[26–28]

The absorption bands were assigned on the basis of the results of TDDFT calculations in acetonitrile, using the structure in Fig. 2, which includes the annulene pendant and a 6-acetyl group that models the effect of the polymer backbone on the electronic structure of the complex, Scheme 1. Using this model, absorption bands are calculated at 573, 373 and 315 nm (with relative intensities 0.04 : 0.8 : 0.04), together with shoulders at 462 and 411 nm. A feature that immediately emerges from the electronic structure calculations is that the molecular orbitals have significant contributions from both the metal and ligand moieties. Labels for the excited states are based here on the two orbitals involved in the electronic transition, Scheme 2. LMCT, ππ′ and dd′ subscripts have been used to indicate the respective sense of the repolarizations rather than the more

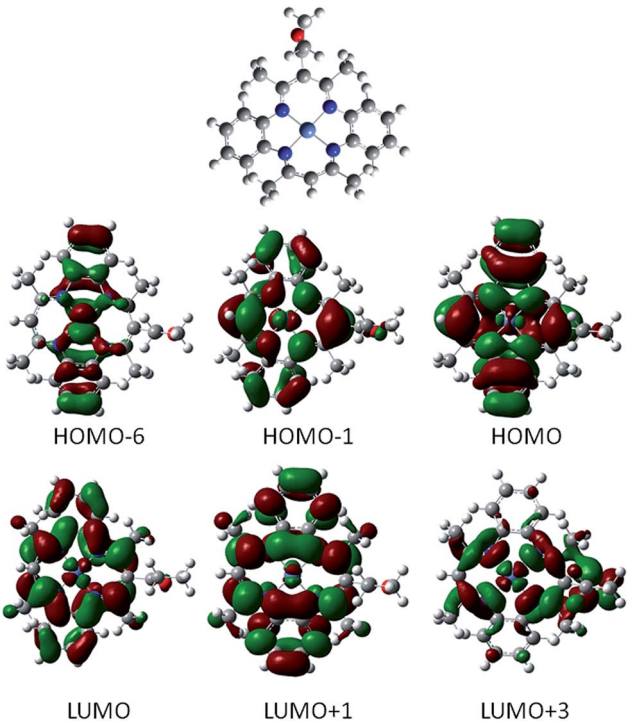

Fig. 2 Molecular orbitals involved in the UV-vis electronic transitions. The optimized structure of the model compound used in the TDDFT calculations is shown at the top of the figure.

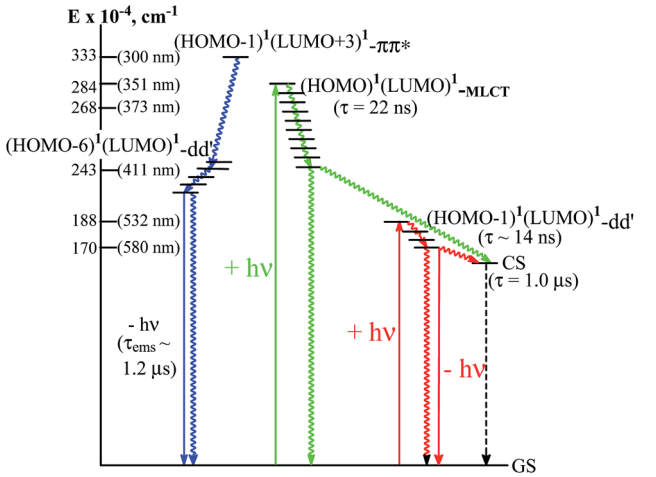

Scheme 2 Simplified energy diagram showing the photophysical processes of [Ni(tmdbzTAA-CO···)] when they are excited with 580, 532 and 351 nm light. A dashed arrow and waved arrows represent respectively the back electron transfer decay of CS reforming the ground state and radiationless relaxations of excited states.

effective displacements of charge occurring in complexes with a higher ionic character.

In addition to the spectroscopic assignments, these calculations were also used to help interpret photochemical processes. Scheme 2 shows the excited states populated by various light excitations. The strong band at 394 nm (calculated 373 nm) is associated with a transition from the HOMO to the LUMO + 1. It brings about a partial transfer from d-electron density to the delocalized π*′ annulene system. Both orbitals involved in the transfer have π electron density, justifying the observed intensity. The excited state populated by this electronic transition is labeled (HOMO)^1(LUMO)^1-MLCT to indicate some degree of charge transfer character in the electronic transition, Fig. 2. Superscripts indicate electrons in the orbital. Electronic transitions from the HOMO − 1 to the LUMO and from the HOMO − 6 to the LUMO (Fig. 2) give rise respectively to the band at 585 and the shoulder at 411 nm. The electronic transitions involve a displacement of the charge that mainly affects the Ni center. They can be regarded as d → d′ transitions with the d orbitals strongly mixed with the ligand π system. The exited states are named as (HOMO − 1)^1(LUMO)^1-dd′ and (HOMO − 6)^1(LUMO)^1-dd′ for future reference. The peak at 300 nm (calculated at 315 nm) has origin in an electronic transition from the HOMO − 1 to the LUMO + 3. While the electronic density in the HOMO − 1 is principally centered on the phenylene groups, it is shifted in the LUMO + 3 over the 5,7-dimethyl-6-carbonyl-4,8-diazapenta-4,6-dienyl group of the annulene ligand. The electronic transition at 300 nm causes a major change in the π density of the ligand and the excited state populated by the transition is then labeled (HOMO − 1)^1(LUMO + 3)^1-ππ*. Another transition to the LUMO + 3 but this time from the HOMO − 6 orbital gives rise to the shoulder at 462 nm. The excited state has a MLCT character and is labeled (HOMO − 6)^1(LUMO + 3)^1-MLCT.

4. Photoprocesses of poly(Ni^{II}[tmdbzTAA])$_2$ in aqueous media

Flash irradiation of poly(Ni^{II}[tmdbzTAA])$_2$ aqueous solutions with visible light, $\lambda_{exc} = 532$ nm, and with ultraviolet light, $\lambda_{exc} = 351$ nm, was used to examine the photobehavior of the polymer. Irradiation at both wavelengths induces some unusual photophysical processes that result in a single charge-separated species.

4a. Species formed and reactivity with 351 nm irradiation. The UV-Vis absorption spectrum of [Ni^{II}(tmdbzTAA-CO$\cdots$)] pendants exhibits an absorption minimum near 351 nm between an intense absorption band with $\lambda_{max} = 390$ nm and a shoulder at 300 nm. Based on the calculations presented above, the 390 and ~300 nm bands are associated with electronic transitions populating respectively the $(HOMO)^1(LUMO)^1$-MLCT and the $(HOMO - 1)^1(LUMO + 3)^1$-$\pi\pi^*$, Scheme 2.

In the 351 nm irradiation of deaerated solutions of poly(Ni^{II}[tmdbzTAA])$_2$ at either pH = 8 or 10, the spectrum, recorded immediately after the laser flash, $t \leq 15$ ns, is shown in the bottom frame of Fig. 3 along with subsequent transient spectra recorded over a millisecond time domain using different delays from the laser flash. In the solution buffered at pH = 10, the changing spectroscopic features reveal that an intermediate, referred to as CS (charge separated), is formed in a short period of time after the laser irradiation, *i.e.*, $t \sim (30 \pm 5)$ ns, and decays on a longer time scale. Moreover, a bleach of the solution in the region between 500 and 650 nm remains at the end of the decay process. This bleach is consistent with a long term photoinduced transformation of the polymer, so that the [Ni^{II}(tmdbzTAA-CO$\cdots$)] pendants are not returned to the condition they had prior to flash irradiation. Oscillographic traces following the decay of the photogenerated absorbance at various wavelengths exhibited two well-defined kinetic steps. Each step was fitted with $\chi^2 \geq 0.978$ to exponentials with rate constants: $k_f = 3.6 \times 10^7$ s^{-1} for the formation of CS and $k_s = 9.5 \times 10^5$ s^{-1} for the decay.

The photochemical behavior of poly(Ni^{II}[tmdbzTAA])$_2$ was also investigated in a 20% (v/v) H_2O in CH_3CN mixed solvent acidified topH = 4 with $HClO_4$. Solutions were aged for 48 h to insure that the slow protonation of the pendants was complete. A transient spectrum with $\lambda_{max} = 438$ nm was promptly generated by the flash irradiation at 351 nm, Fig. 3 top frame. This initially generated spectrum experiences a small change that shifts λ_{max} from 438 nm to 427 nm in a 10^2 ns period after the flash. This spectroscopic transformation, investigated between 380 nm and 450 nm over a 1 μs period, must be assigned to the formation of a transient species from the one promptly formed during the laser flash irradiation. Following formation of this transient, the associated spectrum decays in a time domain of microseconds. Logarithmic plots, ln ξ *vs.* time, are linear and a rate constant, $k = 6.6 \times 10^5$ s^{-1}, is calculated from the slope of the line.

Spectroscopic transformations during photolysis at 351 nm of poly(Ni^{II}[tmdbzTAA])$_2$ solutions buffered at pH = 4, 8 or 10 are attributed to the formation of CS. This charge-separated species is formed from the excited state that has weak charge transfer character, Scheme 2. Assignment as a charge-separated species is based on the redox properties of the pendants revealed in cyclic voltammetry and the observation of related long-lived species in the photolysis of M^{II}[tmdnTAA], M = Ni and Cu.[25] Furthermore, the character of the charge-separated species can be tested by making evident their electron donating and electron accepting reactivity under appropriate thermochemical and kinetic conditions. To confirm the formation of such charge-separated pendants in the 351 nm irradiation of poly(Ni^{II}[tmdbzTAA])$_2$, the polymer was flash irradiated in solutions that also contained electron and hydrogen atom donors, *i.e.*, 0.1 to 1.0 M 2-propanol, 0.1 M NaI ($E^\circ = 1.42$ V *vs.* NHE for the $I^\bullet/I^-$ couple), 0.1 M tEA and 0.1 M tEOA (tEOA = triethanolamine, $E^\circ = 0.82$ V *vs.* NHE for the

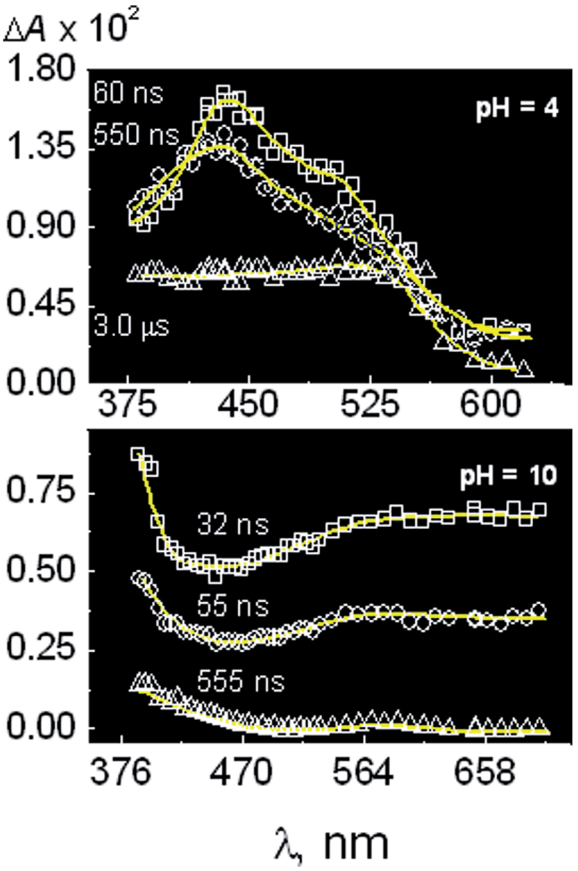

Fig. 3 Transient spectra recorded when solutions of poly(Ni^{II}[tmdbzTAA])$_2$ that contained 1.0×10^{-4} M [Ni^{II}(tmdbzTAA-CO$\cdots$)] pendants buffered respectively at pH = 4 (top frame) and 10 (bottom frame) were flash irradiated at 351 nm. Delays from the laser flash used to record each spectrum and the pH of the solutions are indicated in the figure. In the solution buffered at pH = 10, a spectrum with a maximum at $\lambda_{max} = 646$ nm and another spectroscopic feature with $\lambda_{max} \leq 385$ nm is observed immediately after the laser flash. The position of the 646 nm maximum shifts with time to ~586 nm at the end of the spectroscopic change on the millisecond time domain. A significant change in the intensity of the bands takes place concurrent with the shift of the maximum. Inspection of the absorbance changes at 385 nm, ΔA_{385}, and 547 nm, ΔA_{547}, shows a ratio $\Delta A_{385}/\Delta A_{547} \sim 1.3$ at the end of the flash irradiation and $\Delta A_{385}/\Delta A_{587} \geq 8.4$ at the end of the spectroscopic change.

tEOA$^{\bullet+}$/tEOA couple). The electron-donating reactivity of the charge-separated pendants was investigated using O_2 (E° = −0.33 V *vs.* NHE for the $O_2/O_2^{\bullet-}$ couple) as the electron acceptor.

A common transient spectrum with λ_{max} = 390 nm is generated in the presence (~0.1 M) of tEA, tEOA or 2-propanol, Fig. 4, that has a close resemblance to the spectrum of [Ni^{I}(tmdbzTAA-CO···)]$^-$ pendants generated with the $e_{aq.}^-$ in pulse radiolysis (*vide infra*). Accordingly, the spectrum of the products photogenerated in the presence of tEA, tEOA or 2-propanol is attributed to the formation of reduced [Ni^{I}(tmdbzTAA-CO···)]$^-$ pendants when CS reacts with electron donors. In the reaction with tEA, the formation of [Ni^{I}(tmdbzTAA-CO···)]$^-$ pendants is seen as a process with a pseudo-first order kinetics, $k_{pf} = 1.3 \times 10^7$ s^{-1}. Because 0.1 M tEA was used in the experiment, the rate constant for the second order rate law would be $k = k_{pf}/0.1 = 1.3 \times 10^8$ M^{-1} s^{-1}. The decay of the [Ni^{I}(tmdbzTAA-CO···)]$^-$ pendants takes place with a lifetime τ = 2.3 μs. No reaction was observed with NaI.

The electron-donating reactivity of CS was investigated in aqueous solutions containing 2.2 × 10^{-4} M [Ni^{II}(tmdbzTAA-CO···)] pendants, saturated under 1 atm of O_2 ([O_2] ~5.2 × 10^{-4} M), buffered at pH = 8, and flash irradiated at 351 nm. Transient spectra recorded in a 30 ns to 1 μs time domain were nearly identical to those observed with deaerated solutions. However, different kinetics of the slow step in the decay of the transient spectrum were observed in aerated and deaerated solutions. Instead of the linear plots, ln ξ *vs.* time, calculated for the decay of the transient absorbance in deaerated solutions, the plots ξ^{-1} *vs.* time are linear in the oxygenated solutions. Assuming a second order kinetics on the basis of these results, a ratio of the rate constant to the extinction coefficient, $k/\varepsilon = 6.3 \times 10^5$ cm^{-1} s^{-1}, was calculated from an oscillographic trace recorded at λ_{ob} = 410 nm where the initial change in the absorbance is $\Delta A_0 = 0.094$.

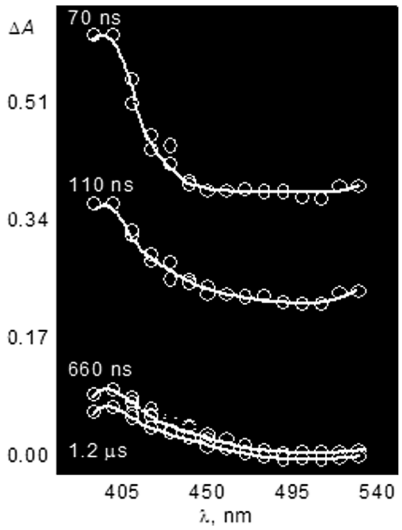

Fig. 4 Transient spectra recorded when a deaerated solution of poly(Ni^{II}[tmdbzTAA])$_2$ buffered at pH = 8 and containing 0.1 M tEA was irradiated at 351 nm.

4b. Species formed and reactivity with 532 nm irradiation. Irradiation of poly(Ni^{II}[tmdbzTAA])$_2$ at 532 nm takes place in the high energy side of the band with λ_{max} ~ 585 nm. Calculations suggest that the absorption band is associated with an electronic transition from the HOMO − 1 to the LUMO. The electronic transition induces some angular repolarization of charge in the Ni center and the populated excited state has been labeled (HOMO − 1)^1(LUMO)^1-dd′, namely an excited state with a weak d–d′ metal-centered character. Transient absorption spectra were recorded after the flash irradiation of a deaerated aqueous solution of the polymer buffered at pH = 8, Fig. 5. Spectra recorded with delays 10 ns < t < 60 ns from the laser flash exhibited a shoulder at 368 nm and bands with λ_{max} ~ 440, 530 and 600 nm. The decay of the spectrum in this time scale was followed at 400 nm and the oscillographic traces collected were fitted to an exponential e^{-kt} with $k = 7.0 \times 10^7$ s^{-1}. In a longer time scale, between 100 and 700 ns, the polymer luminescence has already decayed. Therefore the transient absorption spectrum is not distorted in the 440 nm to 600 nm wavelength region, Fig. 5.

The transient generated in a time scale t < 1 μs when poly(Ni^{II}[tmdbzTAA])$_2$ is flash irradiated at 532 nm is the same CS intermediate generated in the 351 nm photolysis of the polymer. This assignment is based on the similarity of the transient spectrum recorded when the polymer is respectively irradiated at 532 and 351 nm and on the observation that transients generated in either case exhibit the same chemical reactivity toward electron donors and acceptors. It is possible to examine the reactions of the CS photogenerated with 532 nm

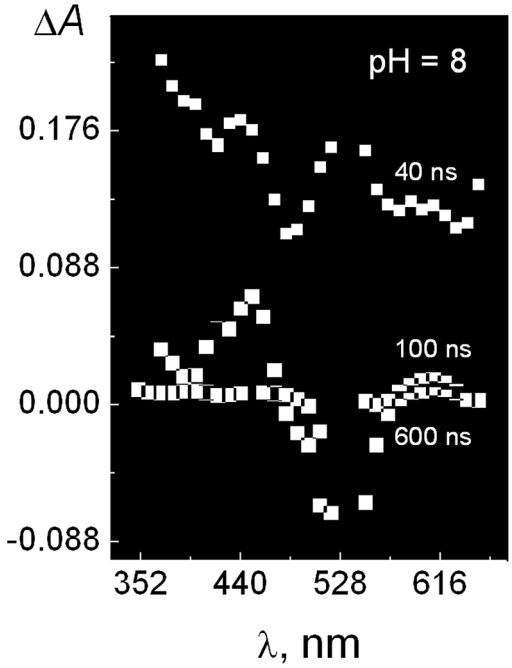

Fig. 5 Transient spectra recorded when a deaerated aqueous solution of the polymer containing 2.2 × 10^{-4} M [Ni^{II}(tmdbzTAA-CO···)] pendants buffered at pH = 8 was flash irradiated at 532 nm. Delays from the laser flash used in these experiments are indicated in the figure.

light using a more extensive range of electron donors and acceptors than those used in the 351 nm irradiations. These redox active species include the electron donors phenol, tEOA, and ferrocene and the electron acceptors $Co^{III}(acac)_3$, $Cu^{II}(acac)_2$ and $Cu^{II}(\beta\text{-alanine})_2$. Flash irradiation of poly(Ni^{II}[tmdbzTAA])$_2$ deaerated solutions containing 2.2×10^{-4} M [Ni^{II}(tmdbzTAA-CO$\cdots$)] pendants and an electron donor, *i.e.*, 1.0×10^{-2} tEOA, 1.0×10^{-2} M or 1.0×10^{-1} M phenol, produces spectra where two new absorption bands, $\lambda_{max} = 375$ and 580 nm, and a bleach of the solution at ~500 nm are observed 100 ns after the flash. A third absorption band with $\lambda_{max} = 430$ nm observed when the photolyzed solution contained phenol is characteristic of the phenoxide radical reported in the literature,[29] and is attributed to the product of the CS reduction by phenol, Fig. 6.

In the presence of oxidants 1.0×10^{-2} M $Co^{III}(acac)_3$, 1.0×10^{-2} M $Cu^{II}(acac)_2$ or 1.0×10^{-2} M $Cu^{II}(\beta\text{-alanine})_2$, flash irradiation of poly(Ni^{II}[tmdbzTAA])$_2$ in deaerated solutions containing 2.2×10^{-4} M [Ni^{II}(tmdbzTAA-CO$\cdots$)]pendants produce on a 12 μs time scale, a transient that is stable on the 6 ms time scale. The same spectrum with maxima at 400 and 600 nm was recorded with any of the electron acceptors using delays from the flash equal to or longer than 30 μs, Fig. 7. It is tentatively assigned to the ligand oxidized species Ni^{II}[(tmdbzTAA$^{\bullet+}$)-CO$\cdots$].

4c. Characterization of [Ni^{I}(tmdbzTAA-CO$\cdots$)]$^-$ pendant transients. The pulse radiolysis technique has been used before to gain information on the species formed in aqueous solution when complexes present as pendants in a polymer react with radiolytically-generated oxidants and reductants.[2,4–6] The technique provides a means to generate chromophores, assigned as [Ni^{I}(tmdbzTAA-CO$\cdots$)]$^-$ pendants for comparison with the flash photolysis experiments, Fig. 4. The radicals $CO_2^{\bullet-}$ ($E^\circ = -1.2$ V *vs.* NHE for the $CO_2/CO_2^{\bullet-}$ couple) and $(CH_3)_2C^{\bullet}OH$ ($E^\circ = -1.2$ V *vs.* NHE for the $(CH_3)_2CO/(CH_3)_2COH^{\bullet}$ couple) as well as the solvated electron, $e_{aq.}^-$ ($E^\circ \sim -2.0$ V *vs.* NHE), were used for the reduction of the [Ni^{II}(tmdbzTAA-CO$\cdots$)] pendants. It must be noted that, according to the cyclic voltammetry experiments, only the reduction potential of $e_{aq.}^-$ is sufficiently negative for the reduction of the nickel(II).

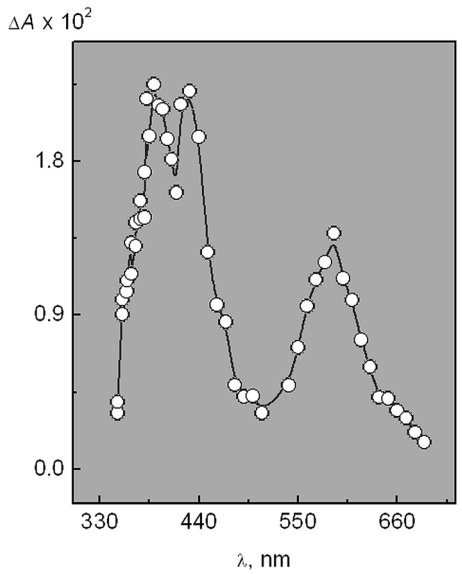

Fig. 6 The 532 nm flash irradiation of a poly[Ni^{II}(tmdbzTAA)]$_2$ solution containing 0.1 M phenol produced the spectrum shown with an absorption band at $\lambda_{max} = 430$ nm assigned to the phenoxide radical.

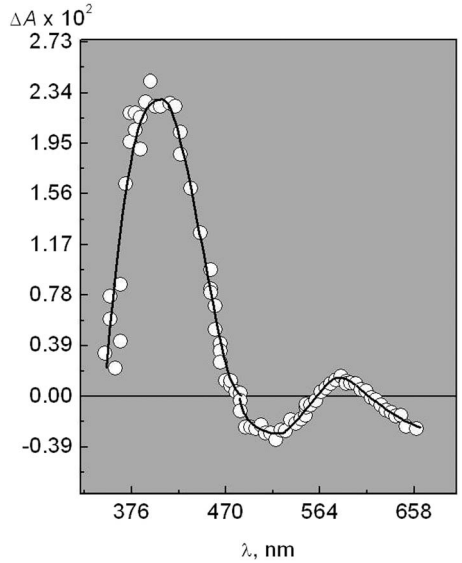

Fig. 7 Transient spectrum recorded when a deaerated solution of poly(Ni^{II}[tmdbzTAA])$_2$ containing an electron acceptor was flash irradiated at 532 nm. The spectrum in the figure was recorded using 1.0×10^{-2} M $Co^{III}(acac)_3$ as the electron acceptor.

When N_2O-saturated solutions of poly(Ni[tmdbzTAA])$_2$ containing 1.0×10^{-2} M $NaHCO_2$ or 2-propanol and 2×10^{-4} M [Ni^{II}(tmdbzTAA-CO$\cdots$)] pendants are pulse radiolyzed, Fig. 8a, $CO_2^{\bullet-}$ and $(CH_3)_2C^{\bullet}OH$ radicals are respectively produced. Both of the radiolytically prepared radicals react with poly(Ni[tmdbzTAA])$_2$ generating spectra with absorption bands having $\lambda_{max} \leq 475$ nm Fig. 8a. Oscillographic traces showing the growth of the spectra at $\lambda_{ob} \sim 400$ and 475 nm and under the regime of a first-order or pseudo-first-order kinetics were fitted with $\chi^2 > 0.9900$ to single exponentials. Different rate constants, $k = 1.7 \times 10^4$ s^{-1} and $k = 8.6 \times 10^3$ s^{-1}, were calculated for the respective reactions of the $CO_2^{\bullet-}$ and $(CH_3)_2C^{\bullet}OH$ radicals. Minimal differences were observed between the spectra of the products respectively generated by the $CO_2^{\bullet-}$ and $(CH_3)_2C^{\bullet}OH$ reactions with the pendants. These transient spectra cannot be assigned to [Ni^{I}(tmdbzTAA-CO$\cdots$)]$^-$ products because reduction potentials of the $CO_2/CO_2^{\bullet-}$ and $(CH_3)_2CO/(CH_3)_2C^{\bullet}OH$ couples are insufficiently negative to drive the reductions of the metal center or other groups in the backbone. Therefore, the spectra shown in Fig. 8a must be associated with species produced either by the coordination of the radicals to the metal center or to the addition of the radicals to the annulene ligand. Calculations of the absorption spectrum of these potential products support the assignments of the transient spectra to chromophores that are adducts of the radicals to the annulene macrocycle, eqn (3) and (4).

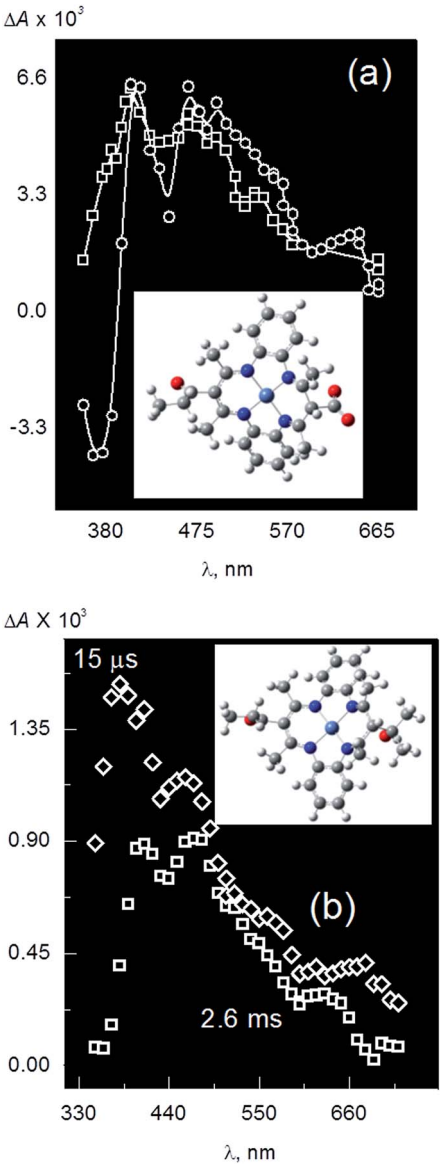

Fig. 8 Spectra recorded in pulse radiolysis when poly(Ni^{II}[tmdbzTAA])$_2$ was reduced: (a), by $CO_2^{\bullet -}$ (○) and $(CH_3)_2C^{\bullet}OH$ (□) and, (b), by the combined actions of $e_{aq.}^-$, and $(CH_3)_2C^{\bullet}OH$. An Inset to (a) and (b) are respectively the optimized structures of the eqn (2) and (3) products. Delays from the radiolytic pulse used recording the spectra are: (○) 500 μs, (□) 300 μs in (a) and (◇) 15 μs, (□) 2.6 ms in (b). Other experimental details are given in the text.

$$\left[Ni^{II}(tmdbzTAA\text{-}CO\cdots)\right] \xrightarrow{CO_2^{\bullet -}} \left[Ni^{II}(O_2C\text{-}tmdbzTAA\text{-}CO^{\bullet}\cdots)\right]^- \quad (3)$$

$$\left[Ni^{II}(tmdbzTAA\text{-}CO\cdots)\right] \xrightarrow{(CH_3)_2C^{\bullet}OH} \left[Ni^{II}((CH_3)_2HO)C\text{-}tmdbzTAA\text{-}CO^{\bullet}\cdots)\right] \quad (4)$$

Optimized structures obtained from the calculations are shown in the insets to Fig. 8a and b respectively, and show that the adducts of the $CO_2^{\bullet -}$ and $(CH_3)_2C^{\bullet}OH$ radicals to the annulene ligand can be regarded as Ni(II)–ligand radical moieties. The spectra calculated for these Ni(II)–ligand radical moieties exhibit the following bands: 770 (736) nm, 650 (630) nm and 573 (563) nm (intraligand charge transfer) and 448 (449) nm, 386 (396) nm ($\pi \rightarrow \pi^*$ transitions) for the respective adducts of $CO_2^{\bullet -}$ and $(CH_3)_2C^{\bullet}OH$ (numbers in parenthesis).

In the radiolysis of N_2-deaerated aqueous solutions of poly-(Ni[tmdbzTAA])$_2$, the $e_{aq.}^-$ and $(CH_3)_2C^{\bullet}OH$ reactants are generated when $(CH_3)_2CHOH$ is the scavenger of the $H^{\bullet}$ and $OH^{\bullet}$ radicals produced by the solvent irradiation. The $(CH_3)_2C^{\bullet}OH$ and $e_{aq.}^-$ are formed in a time scale shorter than 1 μs in the radiolysis of a solution containing 1.0×10^{-4} M $[Ni^{II}(tmdbzTAA\text{-}CO\cdots)]$ pendants and 1.0×10^{-2} M $(CH_3)_2CHOH$. Spectra recorded with delays as short as 15 μs, Fig. 8b (◇), exhibited bands with $\lambda_{max} = 390$ nm and 460 nm. The intensity and positions of these peaks are considerable different of those ($\lambda_{max} = 405$ and 472 nm) observed in the spectrum of the species generated by the $(CH_3)_2C^{\bullet}OH$ radicals alone, Fig. 8a (○). They were attributed to a product of the fast reaction of the pendants with $e_{aq.}^-$. The growth of this product spectrum, nearly ~40 times faster than the observed reaction between the pendants and $(CH_3)_2C^{\bullet}OH$, sets apart the respective reactions of the $(CH_3)_2C^{\bullet}OH$ radical and $e_{aq.}^-$ with $[Ni^{II}(tmdbzTAA\text{-}CO\cdots)]$ pendants. A pseudo-first order rate constant, $k = 3.7 \times 10^5$ s^{-1} was calculated from the absorbance growth at $\lambda_{ob} = 390$ nm for the $e_{aq.}^-$ reaction. Consistent with the reduction of the $[Ni^{II}(tmdbzTAA\text{-}CO\cdots)]$ pendant, a good agreement was found between the spectrum in Fig. 8b (◇) and one calculated from theory for the optimized geometry of $[Ni^{I}(tmdbzTAA\text{-}CO\cdots)]^-$ in water solution. The latter shows the most intense peak at 386 nm generated in a $d \rightarrow \pi^*$ transition, with the d orbital heavily mixed with ligand orbitals of π symmetry. Transitions of lower intensities, at 397 nm, 433 nm, 461 nm and 503 nm shared similar assignments. A peak of lower intensity at 675 nm is associated with $d \rightarrow d'$ transitions that gain intensity through mixing with ligand π orbitals.

On the basis of the previous observations, the formation of $[Ni^{I}(tmdbzTAA\text{-}CO\cdots)]^-$ in the reaction of the pendants with $e_{aq.}^-$ can be represented by the eqn (5).

$$\left[Ni^{II}(tmdbzTAA\text{-}CO\cdots)\right] \xrightarrow{e_{aq.}^-} \left[Ni^{II}(tmdbzTAA\text{-}CO\cdots)\right]^- \quad (5)$$

The Ni(I) product of eqn (5) is unstable and decays in a longer time scale. A spectrum recorded after the decay of this product, Fig. 8b (□), was the same as the spectrum of the adduct of the $(CH_3)_2C^{\bullet}OH$ radical to the annulene ligand, Fig. 8a (□). Oscillographic traces recorded at 380 nm showed that the rate of decay of the $[Ni^{I}(tmdbzTAA\text{-}CO\cdots)]^-$ pendants is kinetically of a first order in the transient concentration. A rate constant, $k_d = 7.7 \times 10^3$ s^{-1}, was calculated from the fitting of the oscillographic traces to an exponential $\xi = \exp(-k_d t)$.

5. $[Ni^{II}(tmdbzTAA\text{-}CO\cdots)]$ luminescence

In contrast to the free Ni^{II}[tmdbzTAA] complex, poly(Ni^{II}[tmdbzTAA])$_2$ exhibits an unusual luminescence under the flash irradiation. This luminescence was investigated with

deaerated solutions of the polymer buffered at pH 8 containing 1.0×10^{-4} M [Ni^{II}(tmdbzTAA-CO···)] pendants. Flash irradiations of the solutions at 532 nm and steady state irradiations at 580 nm produced similar spectra, Fig. 9a. Additionally, a similar luminescence spectrum peaking at 470 nm is recorded when solutions of the polymer are steady state irradiated at wavelengths equal to or shorter than 390 nm. In flash fluorescence experiments, the decay of the emission was followed at 470 nm. Oscillographic traces were fitted to a exponential, $I_o \times \exp(-t/\tau)$, with a lifetime, $\tau = 1.2$ μs.

A particular feature of the luminescence spectrum is that the structured luminescence spans a broad range of wavelengths which encompass wavelengths shorter than those used for the irradiation of the polymer, $\lambda_{exc} = 532$ (flash irradiations) and 580 nm (steady state irradiations), Fig. 9a. Therefore, emitted photons have a higher energy than those used for the excitation of the chromophores. The dependence of the luminescence on the exciting wavelength is reflected in the excitation spectrum, Fig. 9b. It shows that luminescence in the spectroscopic region of the short wavelengths is also induced when the polymer is irradiated at ~330 nm. The upper excited states populated by the 330 nm light must decay to the emissive excited state reached also from the lower lying excited state produced by the 530 or 580 nm light. To explain the formation of the upper emissive excited state at expenses of the lower energy excited states, the latter must acquire additional energy. Because the phenomenon is observed in the irradiations with low and high intensity light, the acquisition of additional energy is likely to occur through an excited state-excited state annihilation process.

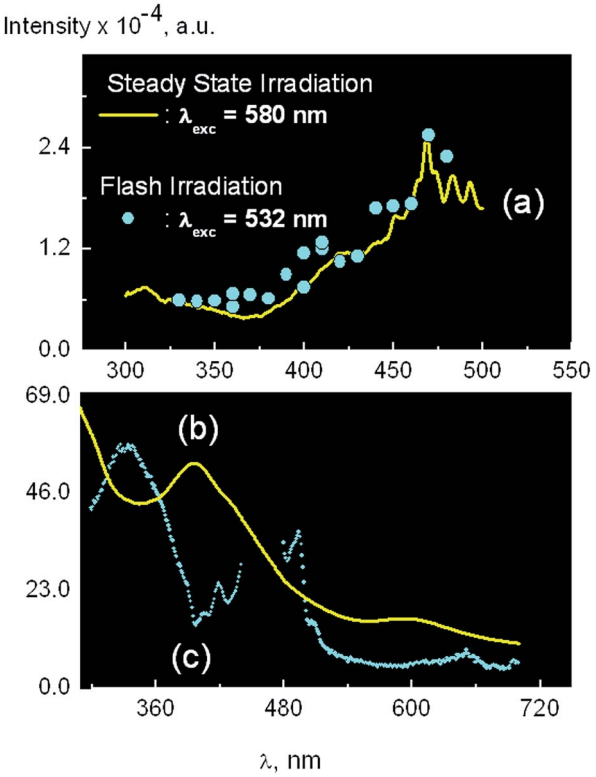

Fig. 9 Luminescence of poly(Ni^{II}[tmdbzTAA])$_2$ in deaerated solutions buffered at pH 8. The emission spectrum, recorded in the steady state irradiation of the solution at $\lambda_{exc} = 580$ nm (a, solid line) has been superimposed with the emission spectrum (a, circles) recorded 5 μs after the flash irradiation of the solution at $\lambda_{exc} = 532$ nm. The excitation spectrum (b) was recorded monitoring the emission at 460 nm. It is superimposed with the absorption spectrum of the solution (c).

Discussion

Grafting the Ni^{II}[tmdbzTAA] complex to poly(isobutylene-*alt*-maleic anhydride) backbone and the subsequent hydrolysis of anhydride groups provides high solubility in H_2O and a strong local concentration of Ni(II) chromophores in the small volume of polymer bundles. As a consequence of these restrained conditions there are significant changes in the thermal and photochemical reactivity of the nickel(II) complex. Migrations of charge and energy within the polymer bundle are observed at light intensities orders of magnitude lower than those required for the observation of the same phenomenon with polymer free complexes. In addition, grafting the macrocyclic complex into the polyelectrolyte backbone provides an opportunity for homogeneous thermal and photochemical catalysis in aqueous media. The test reaction examined in this study is the endoergonic reduction of CO_2 by SO_2 species. The combined antenna and catalytic properties of the polymer facilitate potential applications of poly(Ni[tmdbzTAA])$_2$ driven by the charge separated intermediate CS or the [Ni^{I}(tmdbzTAA-CO···)]$^-$ and Ni^{II}[(tmdbzTAA$^{\bullet+}$)-CO···] pendants.

The reduction of CO_2 in eqn (1), as written is thermodynamically disfavoured by 186.36 kJ mol^{-1}. In aqueous solution at pH = 8, the appropriate reaction, eqn (2), is similarly disfavoured by 70 kJ mol^{-1}. This energetic deficit corresponds to a wavelength for photo-activation of 642 nm.

Studies of photocatalytic behavior carried out with poly(Ni[tmdbzTAA])$_2$ at pH = 8, show high turnover numbers with visible light. The product yield measured at 365 nm is 0.3.

One consequence of the reaction that takes place, eqn (2), is that the pH of the solution gradually decreases and photocatalysis stops when the pH drops below 5, the result of precipitation of the polymer. Photocatalytic activity can be restored by re-dissolution of the polymer at pH 8.

The focus of this study is an examination of the basic morphology of the polymer to understand the effects of pH and the nature of the photocatalytic species.

Modelling bundle morphologies

In large part, the properties of the [Ni^{II}(tmdbzTAA-CO···)] pendants are the result of conditions dictated by the surrounding medium and the disposition of strands in the bundle. The existence of strong interstrand interactions is revealed by the slow change of morphology controlling the protonation of the [Ni^{II}(tmdbzTAA-CO···)] pendants. The diverse interactions that stabilize the different shapes observed in the TEM and AFM micrographs were visualized by short molecular dynamics simulations of small polymer strands (6 repeating units) with

variable protonation states of the carboxylate groups, using the OPLS force field and Macromodel software (Schrodinger). Different protonation states in a single strand, lead to the following observations. Deprotonation of all carboxylates groups in the model generates a linear structure that is retained during the dynamics by internal repulsion of the negative groups. A similar effect results from the modelling of a half-protonated single strand, as adjacent carboxylate groups can form intramolecular H-bonds that prevent bending. However, this may be an artifact of the "single-strand" modelling. Full protonation of the carboxylates generates a structure that bends at the ends, Fig. 10a, or winds into a ball, Fig. 10b, showing intramolecular H-bonds from the carboxylate protons to the annulene nitrogen atoms. The "Texas saddle" structure,[30] characteristic of the latter in its neutral form is distorted by protonation.

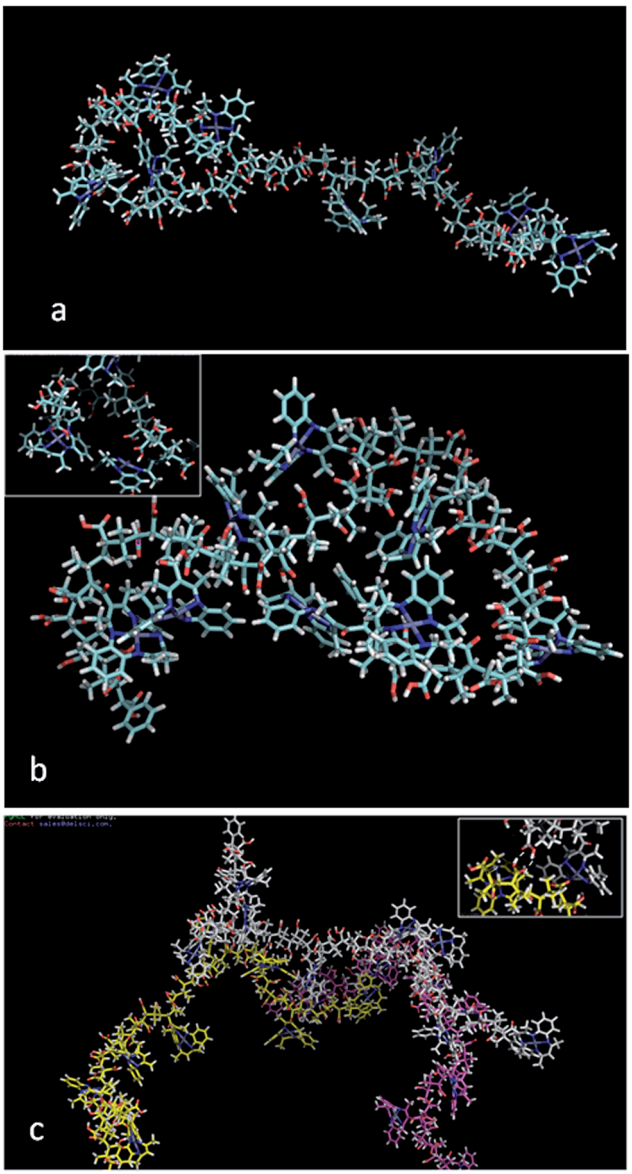

Fig. 10 Structures obtained after short MD simulations of one strand (a and b) and 3 strands (c) for full protonation of the backbone, showing the interactions that help stabilizing a given morphology. The inset in b shows the H-bond interactions between the OH groups of the backbone and the annulene pendant. The inset in c. shows the H-bond interactions between carboxylate groups of different strands.

Aggregation of multiple strands with the conformations described above explain the shapes seen in the micrographs displayed in Fig. S3 and S4.† We also managed to generate a initial 3-strand geometry able to keep the strands together during the MD, Fig. 10c and see a movie showing the oscillatory motions of three strand fragments. When more than one strand is present, the main interactions that glue them together are the interstrand H-bonds between the carboxylate groups, as shown in the figure, although some inter strand H-bonds between protons of carboxylic groups and the annulene N atoms are also observed. Although these results do not provide a quantitative assessment, they allow the potential interactions that can contribute to the observed morphology to be visualized.

Among the factors influencing the change of shape from elongated to globular, a different balance of inter- to intra-strand interactions as shown in Fig. 10a–c has to be considered. Carboxylic acid and carboxylate groups are prone to form H-bond interactions, potentially leading to linear multistrand assemblies when formed between different strands, as shown in Fig. 10c for the case of 3 chains fully protonated (partial deprotonation will reinforce the H-bond interactions). Inter- and intra-strand interactions between protonated carboxylates and deprotonated annulene pendants are more prone to stabilize non-linear structures. As the number of inter-strand interactions increases with concentration, a larger percentage of the carboxylate-annulene pendant interactions favours the formation of non-linear shapes. While the basic medium produces a highly charged backbone, ligand-deprotonation of the [Ni^{II}(tmdbzTAA-CO$\cdots$)] neutralizes the ionic charge (gradually from +2 to +1 and to 0) making the pendants highly hydrophobic. In such conditions, a globular aggregation of strands, as shown in Fig. S4a,† where much ionic charge is directed towards the solvent and the pendants are forced into the interior of the aggregate is favoured over more linear shapes, as shown in Fig. S3.†

Short-lived reaction intermediates

Cyclic voltammetry studies reveal that the oxidation and reduction of [Ni^{II}(tmdbzTAA-CO$\cdots$)] is largely independent of the polymer morphologies and shares similar characteristics to the behavior of [Ni^{II}(tmdbzTAA)] in DMF. The creation of unstable reduced and oxidized derivatives of [Ni^{II}(tmdbzTAA-CO$\cdots$)] pendants in flash photochemical and pulse radiolysis experiments can be interpreted in relation to those generated in cyclic voltammetry. In this case, the irreversibility associated with the removal of one electron from [Ni^{II}(tmdbzTAA-CO$\cdots$)] at 0.75 V, eqn (6), is attributed to the formation of dimers between neighboring oxidized pendants, eqn (7).[27,28]

$$\left[Ni^{II}(\text{tmdbzTAA-CO}\cdots)\right] \xrightarrow{-e^{-}(at+0.75V)} \left[Ni^{II}(\text{tmdbzTAA-CO}^{\cdot}\cdots)\right]^{+} \quad (6)$$

$$2[Ni^{ii}(\text{tmdbzTAA-CO}^{\bullet}\cdots)]^{+} \rightarrow [Ni^{ii}(\text{tmdbzTAA-CO}^{\bullet}\cdots)]_2^{2+} \quad (7)$$

Oxidation of the complex at 1.2 V must be related to the removal of the second electron, eqn (8).

$$\left[\mathrm{Ni^{II}(tmdbzTAA\text{-}CO^{\cdot}\cdots)}\right]^{+} \xrightarrow{-e^{-}\,(at+1.20V)} \left[\mathrm{Ni^{II}(tmdbzTAA\text{-}CO\cdots)}\right]^{2+} \quad (8)$$

It is possible to attribute the irreversibility in the removal of this second electron to the coupling of the reaction in eqn (8) with the redox process,[31] although it is also possible that the removal of the second electron is coupled to the introduction of a keto group into the macrocyclic ligand, as it is illustrated in eqn (9).

$$\left[\mathrm{Ni^{II}(tmdbzTAA\text{-}CO\cdots)}\right]^{2+} \xrightarrow{+H_2O;\ -2H^{-}} \left[\mathrm{Ni^{II}(tmdbzTAA\text{-}CO\cdots)}\right]^{2+} \quad (9)$$

A similar product with a keto group is formed in the air oxidation of the $[Co^{II}(tmdbzTAA)]$ complex.[32]

The one-electron electrochemical reduction of $[Ni^{II}(tmdbzTAA)]$ to $[Ni^{I}(tmdbzTAA)]^{-}$, like the reduction of $[Ni^{II}(tmdbzTAA\text{-}CO\cdots)]$ pendants is an irreversible processes. The $[Ni^{I}(tmdbzTAA\text{-}CO\cdots)]^{-}$ pendants that are produced by the $e_{aq.}^{-}$ in pulse radiolysis, were examined to compare with the products of the electrochemical reduction of the pendants. Calculations show that the pulse radiolysis product has a large fraction of the charge localized on the metal center and to some extent, the product can be regarded as a nickel(I) complex. The instability of $[Ni^{I}(tmdbzTAA\text{-}CO\cdots)]^{-}$ shown in the pulse radiolysis experiments where it is seen to decay with a lifetime $\tau = 1/k_{d} \sim 100$ μs is consistent with the irreversibility of the reduction process in cyclic voltammetry.

Further consideration must be given to the instability of the $[Ni^{I}(tmdbzTAA\text{-}CO\cdots)]^{-}$ and $[Ni^{II}(tmdbzTAA\text{-}CO\cdots^{\cdot})]^{+}$ pendants if they are viable intermediates in catalyzed processes, such as the photocatalyzed reduction of CO_2 where S(IV) species are used as sacrificial reactants. Such reaction intermediates must be scavenged, thereby regenerating the $[Ni^{II}(tmdbzTAA\text{-}CO\cdots)]$ pendants to allow the catalysis to continue to high turnover numbers. Moreover, the scavenging rate must be fast enough to prevent the $[Ni^{I}(tmdbzTAA\text{-}CO\cdots)]^{-}$ and $[Ni^{II}(tmdbzTAA\text{-}CO\cdots^{\cdot})]^{+}$ from entering the reactions that irreversibly degrade the poly(Ni[tmdbzTAA])$_2$. One possible mechanism has the CO product stabilizing the Ni(I) species.

Excited state processes

In photochemical processes the proposed active reagent is the charge separated intermediate, CS, that can react to form the $[Ni^{I}(tmdbzTAA\text{-}CO\cdots)]^{-}$ and $[Ni^{II}(tmdbzTAA\text{-}CO\cdots^{\cdot})]^{+}$ pendants. The energy diagram in the Scheme 2 provides a graphical view of the photochemical pathways available to $[Ni^{II}(tmdbzTAA\text{-}CO\cdots)]$ pendants. Two different photochemical pathways leading to the CS intermediate, are noted, depending on whether the poly(Ni^{II}[tmdbzTAA])$_2$ is irradiated at ~351 nm or 532 nm. The CS intermediate, whose nature will be discussed in the next section, is formed from excited states with different electronic characteristics. The excited state labeled $(HOMO-1)^1(LUMO)^1$-dd′, Scheme 2, is populated by the absorption of 532 nm light. It results from a mixing of metal-centered d′–d with ligand-centered π electron densities. Relative to the ground state, the $(HOMO-1)^1(LUMO)^1$-dd′ excited state shows little if any radial redistribution of charge. Therefore, no transfer of charge from the metal to the ligand or *vice versa* occurs when going from the ground state to the $(HOMO-1)^1(LUMO)^1$-dd′ excited state. Conversely the higher energy $(HOMO)^1(LUMO)^1$-MLCT excited state formed in 351 nm irradiation, mixes some MLCT character into a ligand-centered electronic density.

While the $(HOMO-1)^1(LUMO)^1$-dd′ and $(HOMO)^1(LUMO)^1$-MLCT excited states both result in the formation of the CS, the luminescence of poly(Ni^{II}[tmdbzTAA])$_2$ is more efficient when it is irradiated at 532 or 580 nm. The spectroscopic features of the luminescence are a broad and structured spectrum that spans significantly over wavelengths shorter than the exciting wavelengths, $\lambda_{ex} = 532$ and 580 nm. The structured emission band is characteristic of an emitting excited state with considerable annulene ligand-centered character, and in order to explain the emission of light at wavelengths much shorter than the wavelengths of the absorbed light, an energy accretion mechanism must be invoked. Because the luminescence is seen both in the 532 nm flash irradiations with a high light intensity and 580 nm steady state irradiations with a low light intensity, it cannot be associated with the sequential absorption of two photons. The experimental observation can be rationalized by a mechanism that involves the excited state-excited state annihilation to produce an emissive $(HOMO-6)^1(LUMO)^1$-dd′ excited state, eqn (10) and (11).

$$\left[\mathrm{Ni^{II}(tmdbzTAA\text{-}CO\cdots)}\right] \xrightarrow[\lambda_{exc}=532nm]{+h\nu} (HOMO-1)^1(LUMO)^1{}_{-dd'}\left[\mathrm{Ni^{II}(tmdbzTAA\text{-}CO\cdots)}\right] \quad (10)$$

$$2(HOMO-1)^1(LUMO)^1{}_{-dd'}\left[\mathrm{Ni^{II}(tmdbzTAA\text{-}C=O\cdots)}\right] \rightarrow \left[\mathrm{Ni^{II}(tmdbzTAA\text{-}C=O\cdots)}\right] + (HOMO-6)^1(LUMO)^1{}_{-dd'}\left[\mathrm{Ni^{II}(tmdbzTAA\text{-}C=O\cdots)}\right] \quad (11)$$

Similar excited state-excited state annihilation processes have been observed in the photolysis of $Re(CO)_3$(1,10-phenanthroline)$^{+}$ bonded to poly-(vinylpyridine)$_{600}$ and a polyimide containing pendant Al^{III}phthalocyaninetetrasulfonate groups, $[HOAl^{III}(pc)(SO_3^{-})_3(SO_2N<)]^{3-}$.[2,33] If energy migration through

the bundle brings two electronically excited pendants to the contact distance, an exciplex could be formed before the products of eqn (10). An alternative mechanism for the excited state – excited state annihilation involves Förster–Dexter[34] energy transfers. Energy migration through the bundle needs only to bring the excited pendants to a distance where the rate of energy transfer equals the rate of spontaneous decay of the excited state.

Inspection of the excitation spectrum in Fig. 8 reveals that the excited state annihilation process, eqn (9) and (10), justifies the induced emission when $\lambda_{ex} = 532$ nm but does not account for the intense luminescence observed when poly(Ni[tmdbzTAA])$_2$ solutions are irradiated at wavelengths $\lambda_{ex} < 400$ nm. Given the ~330 nm position of the maximum in the excitation spectrum, there must be an upper excited state that converts with a significant yield to the emissive (HOMO − 6)^1(LUMO)^1-dd′ excited state populated by the excited state annihilation process, eqn (9) and (10) and Scheme 2. On the basis of the calculated energies of the excited states, it is likely that the upper excited state is the (HOMO − 1)^1(LUMO + 3)^1-dd′. This assignment is consistent with the assignment of the ~330 nm shoulder in the absorption spectrum of the pendant to the electronic transition from the ground state to the (HOMO − 1) 1(LUMO + 3)^1-dd′, Fig. 2. No evidence was found that the CS intermediate is formed in the decay of the (HOMO − 1)1(LUMO + 3)^1-dd′.

Photogeneration and nature of CS

The conversion of the (HOMO − 1)^1(LUMO)^1-dd′ excited state to the CS intermediate is slightly faster than the analogous conversion from the (HOMO)^1(LUMO)^1-MLCT where the electronic density has been repolarized. Two mechanisms can account for this counter-intuitive observation. In one of these mechanisms, the (HOMO)^1(LUMO)^1-MLCT and the (HOMO − 1)^1(LUMO)^1-dd′ excited states converts to the CS by parallel paths, Scheme 2. The decay rate of the (HOMO)^1(LUMO)^1-MLCT and the (HOMO − 1)^1(LUMO)^1-dd′ excited states are determined by the respective sums of rate constants for the non-radiative relaxation to the ground state, for conversion to the CS, and in the (HOMO − 1)^1(LUMO)^1-dd′ case, the upper energy conversion to the (HOMO − 6)^1(LUMO)^1-dd′ excited state. A slightly larger sum of the (HOMO − 1)^1(LUMO)^1-dd′ rate constants results in faster formation of CS from this excited state. Since CS is formed with approximately the same efficiency from both excited states, the rate constant for the conversion of the (HOMO − 1)^1(LUMO)^1-dd′ needs to be almost twice the value of the rate constant for the (HOMO)^1(LUMO)^1-MLCT conversion to the CS intermediate. In the second mechanism, the (HOMO)^1(LUMO)^1-MLCT excited state converts to the (HOMO − 1)^1(LUMO)^1-dd′ excited state and the latter will be the only one of the two excited states forming the CS. To explain the slower rate of CS formation from the (HOMO)^1(LUMO)^1-MLCT one has to assume that the conversion of the latter to the (HOMO − 1)^1(LUMO)^1-dd′ is slowing the overall process. If this were the mechanism, a luminescence as intense as in the steady state irradiation at $\lambda_{exc} > 532$ nm, where the (HOMO − 1)^1(LUMO)^1-dd is populated, would be observed. However, inspection of the absorption and excitation spectra in Fig. 8b and c, shows that the intensity of the luminescence has a minimum in a region of wavelengths were mainly the (HOMO)^1(LUMO)^1-MLCT is photogenerated. To shorter wavelengths, $\lambda_{ex} < 350$ nm equivalent to $E > 286 \times 10^4$ cm^{-1} in Scheme 2, a more intense luminescence is observed when the (HOMO − 1)^1(LUMO + 3)^1-ππ* excited state, instead of the (HOMO)^1(LUMO)^1-MLCT, is preferentially populated.

Intermediates in the photolysis of M(tmdnTAA), M = Cu(II) and nickel(II), were tentatively assigned as charge separated species in a previous study,[25] and based on the experimental observations presented in this work, a similar assignment is made for CS. Indeed, the dual reactivity of the intermediate with electron donors and acceptors can only be rationalized if CS has a structure possessing some kind of charge separation. Such charge separation can be that of a biradical or a nickel(I)–ligand radical intermediate, [Ni^{I}[(tmdbzTAA$^{\bullet+}$)-CO···]. A biradical structure requires that different charge be localized in different groups of the annulene ligand with little if any change in the electronic density of the metal center. In contrast, the metal center in [Ni^{I}[(tmdbzTAA$^{\bullet+}$)-CO···] has increased its charge at expenses of the ligand. The transient spectra recorded when CS reacts with electron donors are identical to the spectrum of the [Ni^{I}[(tmdbzTAA)-CO···]$^-$ produced when [Ni^{II}(tmdbzTAA-CO···)] pendants are reduced by the $e_{aq.}^-$ in pulse radiolysis, and so [Ni^{I}(tmdbzTAA-CO···)]$^-$, is formed in the reduction of CS. In contrast, reduction of a biradical structure will form a ligand–radical instead than the [Ni^{I}[(tmdbzTAA)-CO···]$^-$ complex, justifying the assignment of a nickel(I)–ligand radical structure to CS.

Conclusions

The grafting of the nickel(II) annulene complex to the poly(isobutylene-*alt*-maleic anhydride) backbone provided macrocyclic complex pendants with an enhanced pH-dependent solubility in a broad range of solvents. Furthermore, the nickel(II) complex exhibits novel thermal and photochemical reactions in aqueous media. Among them, the hindered protonation of the pendants, the upper conversion of photonic energy, the photogeneration of reactive charge-separated moieties should be highlighted. The possibility of performing these reactions in diverse media allows the use of the complex in practical applications such as in the homogeneous catalysis of chemical reactions in aqueous media or as components of optical devices. In this work, the capability of the pendants to function in the dual role of antenna and catalyst of reactions applicable to the storage of energy has been exemplified with the CO_2 photoreduction to CO with S(IV) species acting as sacrificial reagents.

Acknowledgements

Part of this work was carried out in the Notre Dame Radiation Laboratory (NDRL). The NDRL is supported by the Division of Chemical Sciences, Geosciences and Biosciences, Basic Energy

Sciences, Office of Science, United States Department of Energy through grant number DE-FC02-04ER15533. This is contribution number NDRL 4952. G.T.R thanks to CONICET for funding (PIP 0389) and Department of Chemistry of Notre Dame University for funding and hosting him there. G.T.R and C.V. are Research Members of CONICET (Argentina). J.C. thanks FONDECYT, CONICYT, Chile project #1100773.

References

1 (*a*) A. Gasnier, C. Bucher, J.-C. Moutet, G. Royal and E. S.-A. Pierre Terech, *Macromol. Symp.*, 2011, **304**, 87–92; (*b*) S.-J. Liu, Y. Chen, W.-J. Xu, Q. Zhao and W. Huang, *Macromol. Rapid Commun.*, 2012, **33**, 461–480; (*c*) W. Y. Tam, C. S. K. Mak, Ng. A. M. Ching, A. B. Djurišić and W. K. Chan, *Macromol. Rapid Commun.*, 2009, **30**, 622–626; (*d*) C. A. Fustin, P. Guillet, U. S. Schubert and J. F. Gohy, *Adv. Mater.*, 2007, **19**, 1665–1673; (*e*) S. J. Buwalda, P. J. Dijkstra and J. Feijen, *J. Polym. Sci., Part A: Polym. Chem.*, 2012, **50**, 1783–1791; (*f*) A. L. Lewis and J. D. Miller, *Polymer*, 1993, **34**, 2453–2457; (*g*) M. Kaneko and E. Tsuchida, *J. Polym. Sci., Polym. Chem. Ed.*, 1981, **16**, 397–522; (*h*) B. Happ, C. Friebe, A. Winter, M. D. Hager and U. S. Schubert, *Eur. Polym. J.*, 2009, **45**, 3433–3441; (*i*) S. Schmatloch, A. M. J. Van Den Berg, A. S. Alexeev, H. Hofmeier and U. S. Schubert, *Macromolecules*, 2003, **36**, 9943–9949.

2 G. T. Ruiz, A. G. Lappin and G. Ferraudi, *J. Photochem. Photobiol., A*, 2009, **206**, 1–9.

3 (*a*) G. Ferraudi, G. Estiu, A. G. Lappin, M. Villagran, J. P. Muena, J. Costamagna and J. H. Zagal, *Helv. Chim. Acta*, 2009, **92**, 339–356; (*b*) M. Villagran, J. P. Muena, G. Ferraudi, J. H. Zagal and J. Costamagna, *J. Coord. Chem.*, 2009, **62**, 141–149, and references therein.

4 S. Thomas, G. T. Ruiz and G. Ferraudi, *Macromolecules*, 2006, **39**, 6615–6621.

5 G. T. Ruiz, A. G. Lappin and G. Ferraudi, *J. Porphyrins Phthalocyanines*, 2010, **14**, 69–80.

6 G. T. Ruiz, A. G. Lappin and G. Ferraudi, *J. Polym. Sci., Part A: Polym. Chem.*, 2012, **50**, 2507–2515, and references therein.

7 J. Guerrero, O. E. Piro, E. Wolcan, M. R. Feliz, G. Ferraudi and S. A. Moya, *Organometallics*, 2001, **20**, 2842–2853.

8 A. A. Frost and R. G. Pearson, *Kinetics and Mechanism*, John Wiley & Sons, New York, 1953.

9 E. E. Wegner and A. J. Adamson, *J. Am. Chem. Soc.*, 1962, **84**, 2411.

10 S. K. Dutta and G. Ferraudi, *J. Phys. Chem. A*, 2001, **105**, 4241–4247.

11 G. L. Hug, Y. Wang, C. Schöneich, P.-Y. Jiang and R. W. Fessenden, *Radiat. Phys. Chem.*, 1999, **54**, 559–566.

12 G. V. Buxton, C. L. Greenstock, W. P. Hellman and A. B. Ross, *J. Phys. Chem. Ref. Data*, 1988, **17**, 513–886.

13 M. J. Frisch, G. W. Trucks, H. B. Schlegel, G. E. Scuseria, M. A. Robb, J. R. Cheeseman, G. Scalmani, V. Barone, B. Mennucci, G. A. Petersson, H. Nakatsuji, M. Caricato, X. Li, H. P. Hratchian, A. F. Izmaylov, J. Bloino, G. Zheng, J. L. Sonnenberg, M. Hada, M. Ehara, K. Toyota, R. Fukuda, J. Hasegawa, M. Ishida, T. Nakajima, Y. Honda, O. Kitao, H. Nakai, T. Vreven, J. A. Montgomery Jr, J. E. Peralta, F. Ogliaro, M. Bearpark, J. J. Heyd, E. Brothers, K. N. Kudin, V. N. Staroverov, R. Kobayashi, J. Normand, K. Raghavachari, A. Rendell, J. C. Burant, S. S. Iyengar, J. Tomasi, M. Cossi, N. Rega, J. M. Millam, M. Klene, J. E. Knox, J. B. Cross, V. Bakken, C. Adamo, J. Jaramillo, R. Gomperts, R. E. Stratmann, O. Yazyev, A. J. Austin, R. Cammi, C. Pomelli, J. W. Ochterski, R. L. Martin, K. Morokuma, V. G. Zakrzewski, G. A. Voth, P. Salvador, J. J. Dannenberg, S. Dapprich, A. D. Daniels, Ö. Farkas, J. B. Foresman, J. V. Ortiz, J. Cioslowski and D. J. Fox, *Gaussian 09*, Revision A.1, Gaussian, Inc., Wallingford CT, 2009.

14 A. D. Becke, *J. Chem. Phys.*, 1993, **98**, 5648–5652.

15 C. Lee, W. Yang and R. G. Parr, *Phys. Rev. B: Condens. Matter Mater. Phys.*, 1988, **37**, 785–789.

16 P. J. Stephens, F. J. Devlin, C. F. Chablowski and M. Frisch, *J. Phys. Chem.*, 1994, **98**, 11623–11627, and references therein.

17 The results have been compared with those derived using the M06 functional (ref) for both the geometry optimization and TDDFT calculations. Better agreement with experiment was obtained in this case with B3lyp.[27]

18 J. Denis, P. Eric, C. Llaria, A. Carlo, V. Rosendo, Z. Yan and T. Donald, On the performances of the M06 Family of Density Functionals for electronic excitation energies, *J. Chem. Theory Comput.*, 2010, **6**, 2071–2085.

19 W. J. Hehre, L. Radom, P. V. R. Schleyer and J. A. Pople, *Ab Initio Molecular Orbital Theory*, John Wiley & Sons, New York, 1986.

20 (*a*) P. J. Hay and W. R. Wadt, *J. Chem. Phys.*, 1985, **82**, 270–283; (*b*) P. J. Hay and W. R. Wadt, *J. Chem. Phys.*, 1985, **82**, 299–313.

21 J. B. Foresman, T. A. Keith, K. B. Wiberg, J. Snoonian and M. J. Frisch, *J. Phys. Chem.*, 1996, **100**, 16098–16104.

22 *Suite 2011: MacroModel*, version 9.9, Schrödinger, LLC, New York, NY, 2011.

23 V. L. Goedken and M. C. Weiss, *Inorg. Synth.*, 1980, **20**, 15–19.

24 I. Manners, *Science*, 2001, **294**, 1664–1666.

25 J. Costamagna, G. Ferraudi, M. Villagran and E. Wolcan, *J. Chem. Soc., Dalton Trans.*, 2000, 2631–2637.

26 C. L. Bailey, R. D. Bereman, D. P. Rillema and R. Nowak, *Inorg. Chem.*, 1986, **25**, 933–938.

27 P. J. Hochgesang and R. D. Bereman, *Inorg. Chim. Acta*, 1988, **149**, 69–76.

28 A. Deronzier and M.-J. Marques, *Electrochim. Acta*, 1994, **3l9**, 1377–1383.

29 (*a*) G. E. Adams, B. D. Michael and E. J. Land, *Nature*, 1966, **211**, 293–294, DOI: 10.1038/211293a0; (*b*) G. Dobson and L. I. Grossweiner, *Radiat. Res.*, 1964, 708–714.

30 (*a*) F. A. Cotton and J. Czuchajowska, *Polyhedron*, 1990, **9**, 2553–2566; (*b*) P. Mountford, *Chem. Soc. Rev.*, 1998, **27**, 105–115.

31 A. J. Bard and L. R. Faulkner, *Electrochemical Methods. Fundamentals and Applications*, John Wiley & Sons, N. Y., 1980.

32 M. C. Weiss and V. Goedken, *J. Am. Chem. Soc.*, 1976, **98**, 3389–3392.
33 (*a*) E. Wolcan and G. Ferraudi, *J. Phys. Chem. A*, 2000, **104**, 9281–9286; (*b*) E. Wolcan and M. R. Feliz, *Photochem. Photobiol. Sci.*, 2003, **2**, 412–417; (*c*) E. Wolcan, G. Ferraudi, M. R. Feliz, R. V. Gomez and L. Mickelsons, *Supramol. Chem.*, 2003, **15**, 143–148; (*d*) M. R. Feliz and G. Ferraudi, *Inorg. Chem.*, 2004, **43**, 1551–1557.
34 G. Ferraudi, Flash Photolysis and Chemistry of Transients and Excited States, in *Physical Inorganic Chemistry, Principles, Methods and Models*, ed. A. Bakaac, Wiley, New Jersey, 2010, ch. 6, pp. 226–233 and references therein.